Materials Science, Vol. 21, No. 1, 2003

Structure analysis and local magnetic parameters of magnetoresistance tunnel junctions

CHEOLGI KIM [1*], CHONG-OH KIM[1], YONGKANG HU[1],
JAROSŁAW KANAK[2], TOMASZ STOBIECKI[2], SATOSHI OGATA[3],
MASAKIYO TSUNODA[3], MIGAKU TAKAHASHI[3]

[1]Department of Materials Engineering, Chungnam National University, Taejon, 305-764, Korea

[2]Department of Electronics, University of Mining and Metallurgy, 30-059 Krakow, Poland

[3]Department of Electronic Engineering, Tohoku University, Sendai 980-8579, Japan

The Magnetic Tunnel Junctions (MTJs) were deposited by DC magnetron sputtering method in the following layer sequence: Ta(50 Å)/Cu(100 Å)/Ta(50 Å)/$Ni_{80}Fe_{20}$(20 Å)/Cu(50 Å)/$Mn_{75}Ir_{25}$(100 Å) /$Co_{70}Fe_{30}$(25 Å)/Al-O/$Co_{70}Fe_{30}$(25 Å)/$Ni_{80}Fe_{20}$(*t*)/Ta(50 Å)/, with t = 0 Å, 100 Å and 1000 Å. X-ray diffraction analysis revealed that highly oriented *fcc* (111) of $IrMn_3$, Cu, $Ni_{80}Fe_{20}$ and $Co_{70}Fe_{30}$ crystal planes are stacked parallel to the substrate plane. An improvement of (111) texture and crystallinity was observed after annealing. The tunneling magnetoresistance ratio of patterned junction with electrode layer of $Ni_{80}Fe_{20}$ (t = 1000 Å) deposited on the free layer of $Co_{70}Fe_{30}$ (25 Å) exceeds 40% at a room temperature after annealing at 200 °C in the magnetic field of 1 kOe. Local hysteresis loops were measured using the magneto-optical Kerr effect system. Relatively irregular variations of the coercive force H_c and unidirectional anisotropy field H_{ua} in as-deposited sample are revealed. After 200 °C annealing, the H_c decreases but H_{ua} increases with smooth local variations. Two-dimensional plots of H_c and H_{ua} show symmetric saddle shapes with their axes aligned with the pinned layer. The distribution of surface roughness is symmetric with respect to the centre of MTJ. Correlation between surface roughness and the variation of H_{ua} suggests that the H_{ua} variation of the free layer is well described by dipole interactions in the form of so-called Néel "orange peel" coupling.

Key words: *coercive force; exchange coupling; TMR; XRD; MOKE; surface roughness*

1. Introduction

Ever since large tunnel magnetoresistance (TMR) at a room temperature was observed [1, 2], properties of magnetic tunnel junctions (MTJs) have been steadily

[*]Corresponding author, e-mail: cgkim@cnu.ac.kr.

improved. Recently MTJs with 60% TMR at a room temperature (RT) have been demonstrated [3]. This fact makes them appropriate for magnetic random access memory (M-RAM) devices [4, 5], highly sensitive bio-sensors [6, 7] or read heads in hard-disk drives [8].

As is generally known [9, 10], the tunneling resistance (R) depends on the relative orientation of the magnetization (M) of each layer. In a memory device, an independent switching of the magnetically soft layer is achieved by making the other layer either exchange-biased or magnetically hard. The antiparallel and parallel M arrangements in a tunnel junction may represent two states of a bit. Reading the information requires only the measurement of R. Writing the information involves a switching of M for one layer, ideally without affecting M for the reference layer.

To stabilize the reference layer, its hysteresis loop can be shifted away from the zero field by exchange biasing. M of the reference layer is pinned to an adjacent antiferromagnetic (AF) layer through an exchange interaction, which effectively acts as internal field on the reference layer and must be overcome in order to switch the layer.

The magnetization reversal in a stack of thin films may be strongly affected by various magnetic parameters. One important parameter is unidirectional anisotropy of free layer caused by the interlayer coupling between pinned and free layers separated by an insulating spacer. The main interlayer coupling effects have been identified to be RKKY-like coupling through an indirect exchange mediated by the itinerant electrons, and Néel's "orange peel" coupling from magnetic dipole interaction related to interfacial morphological corrugations [11–14]. When an insulating layer prevents electron itinerancy, dipole interaction is reasonable rather than RKKY-like coupling.

However, there are contradictory results for the correlation between exchange coupling and surface roughness; while one result indicates that the exchange coupling is inversely proportional to surface roughness [15, 16], the other claims that the exchange coupling is proportional to surface roughness [17]. A full understanding of their relationship has not been attained because of the complex material and magnetic parameters.

In reality, the inhomogeneity of material and structure are responsible for the above results, hence local magnetic parameters (magnetization, coercivity and unidirectional anisotropy field) in both free and pinned layers can be non-uniform over the junction.

The distribution of magnetic parameters probably arises from local variations of the magnetic anisotropy and/or coupling from grain to grain within each layer. The magnetization reversal and strength of exchange coupling play a decisive role in the magnetoresistivity (MR) ratio and its field sensitivity [18, 19].

In this work, we investigate not only general properties of the structure and magnetoresistance, but also distributions of the coercive force, unidirectional anisotropy field and surface roughness on patterned junctions prepared by DC-sputtering method. We discuss magnetic parameters obtained and coupling interactions in relation to the surface roughness.

2. Experimental

MTJs with the structure of Ta(50 Å)/Cu(100 Å)/Ta(50 Å)/$Ni_{80}Fe_{20}$(20 Å) /Cu(50 Å)/$Mn_{75}Ir_{25}$(100 Å)/$Co_{70}Fe_{30}$(25 Å)/Al-O/$Co_{70}Fe_{30}$(25 Å)/$Ni_{80}Fe_{20}$(*t*)/Ta(50 Å), and the thickness of $Ni_{80}Fe_{20}$ top electrode of t = 0 Å, 100 Å and 1000 Å (Fig. 1), were deposited on thermally oxidized Si wafers using DC magnetron sputtering with ultra pure Ar (9N) as a process gas, in a chamber with a base pressure of 3×10^{-9} Torr. For barrier formation, metallic Al film of 15 Å thickness was deposited and subsequently oxidized in an oxidation chamber with a radial line slot antenna (RLSA) for 2.45-GHz microwaves [3]. Kr was used as the inert gas mixed with O_2 molecular gas for the plasma oxidation. For the X-ray diffraction and VSM measurements, in the same deposition process simultaneously the samples in the form of discs of 10 mm in diameter were fabricated. In-situ patterned junctions were prepared using a shadow mask during deposition. The junction size was 180×180 μm^2 or 250×250 μm^2.

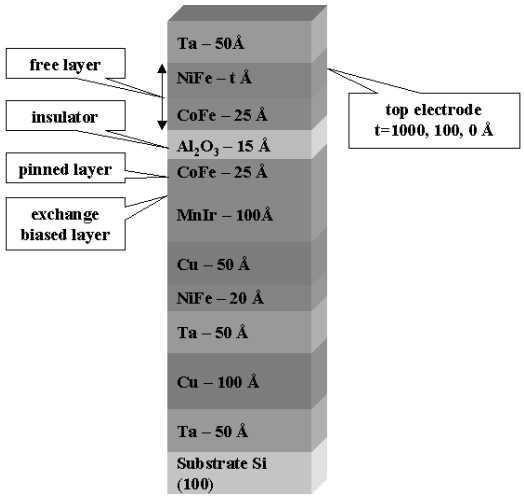

Fig. 1. Multilayer structure of MTJ

The junction samples were annealed at 200 °C for 1 hour under the magnetic field of 1 kOe, followed by field cooling. The magneto-optical Kerr effect (MOKE) method was used to obtain the local *M–H* loops under a 50 Hz driving magnetic field with 100 Oe amplitude. The penetration depth of He–Ne laser light is about 20 nm, which is enough to affect the whole thickness of the free layer. The field was applied in the annealing field direction. The laser beam size was about 2 μm in diameter, corresponding to the spatial resolution of the micro-MOKE system. The sample was scanned using a computer-controlled *x–y* stage to obtain a two-dimensional plot of magnetic parameters. The distribution of the surface roughness was determined by atomic force microscopy (AFM) at different points across the junction.

3. Results and discussion

3.1. Structure

In order to understand the different magnetic performances in as-deposited and annealed MTJs, an X-ray diffraction experiment was done in θ–2θ geometry for low

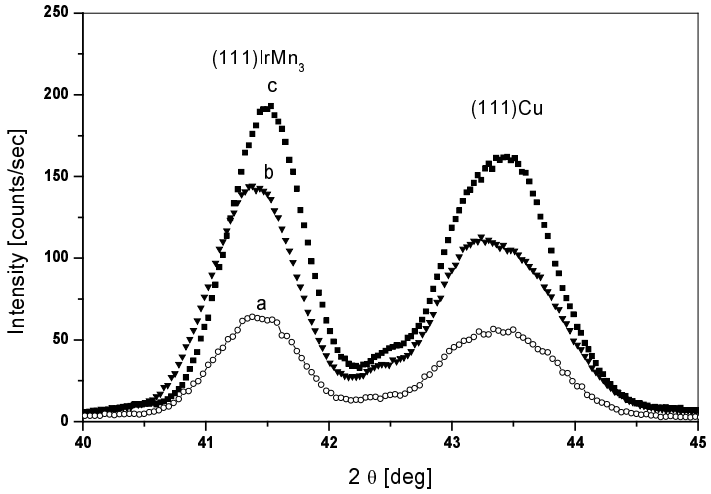

Fig. 2. Textured part of θ–2θ profile with *fcc* (111) $IrMn_3$, (111) Cu planes for as-deposited samples with free layer of $Co_{70}Fe_{30}$(25 Å) (a), $Co_{70}Fe_{30}$(25 Å)/$Ni_{80}Fe_{20}$ (t = 100 Å) (b) and annealed $Co_{70}Fe_{30}$(25 Å)/$Ni_{80}Fe_{20}$ (t = 100 Å) (c)

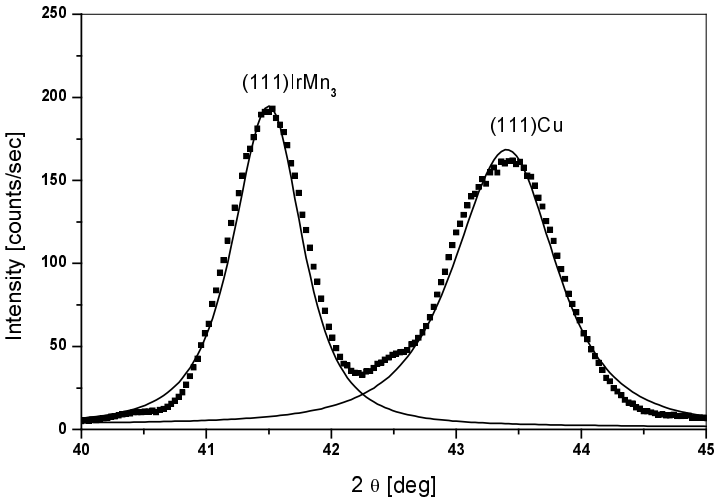

Fig. 3. θ–2θ profile for annealed samples of $Co_{70}Fe_{30}$(25 Å)/$Ni_{80}Fe_{20}$ (t = 100 Å) with fitting lines of *fcc*-(111) $IrMn_3$ and (111) Cu peaks

and high angles using a Philips diffractometer of the type X'Pert–MPD with Cu-anode (λ_{Cu} = 1.54184 Å). Figure 2 shows the high angle diffraction θ–2θ scan for the as-deposited and annealed stacking structure of the samples with the thickness of NiFe t = 0 Å and 100 Å. According to the diffraction data of Tsunoda [22], strong *fcc* peaks of (111) $IrMn_3$ and (111) Cu (not distinguished with *fcc* (111) $Ni_{80}Fe_{20}$ and $Co_{70}Fe_{30}$) are observed. These peaks manifested highly oriented *fcc* (111) crystal planes stacked parallel to the film plane. Lattice planes and lattice constants were determined from these peaks positions for as-deposited and annealed samples (as for example, Fig. 3). These parameters of *fcc*-(111) $IrMn_3$ and *fcc*-(111) Cu for the samples with the thickness of $Ni_{80}Fe_{20}$ t = 0 Å and 100 Å are: (111) $IrMn_3$ d = 2.179 Å (a = 3.775 Å) and d = 2.181 Å (a = 3.777 Å), respectively and for (111) Cu d = 2.085 Å (a = 3.612 Å) and d = 2.087 Å (a = 3.614 Å), respectively. The annealing treatment in vacuum at 200 °C for 1 hour induces an increase in (111) peaks intensity and a slight peak shift to higher 2θ position: (111) $IrMn_3$ d = 2.176 Å (a = 3.768 Å) and (111) Cu d = 2.084 Å (a = 3.610 Å) indicate an improvement in the crystallinity [22, 23] of the multilayer structure.

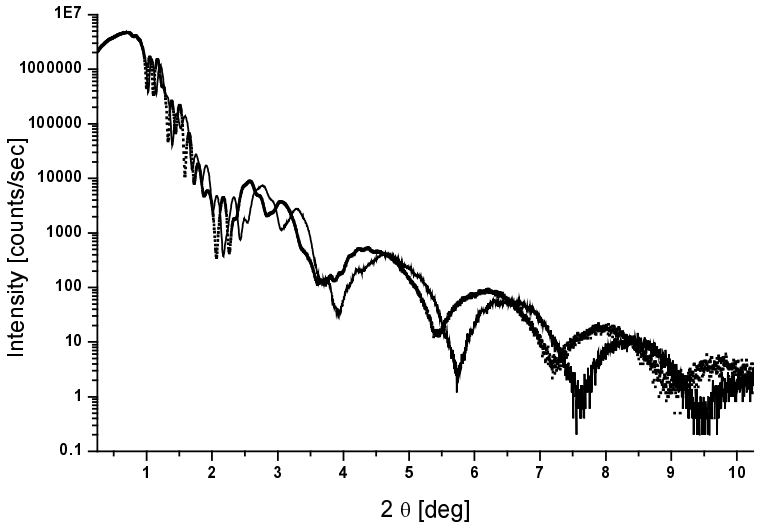

Fig. 4. The low angle diffraction θ–2θ reflectivity profiles of as-deposited (solid line) and annealed (points) samples

The low-angle diffraction (scan θ–2θ) in the range of $2\theta < 10°$ presents the reflectivity curves (Fig. 4) of as-deposited and annealed samples. No remarkable differences (within the accuracy of this experiment) were recognized in these curves (Fig. 4), meaning that no significant changes occurred in the interfacial roughness. The shift of reflectivity curve of annealed sample to the lower angle of 2θ indicates particularly an increase of the thickness of the Ta sublayer. Tantalum, due to twice higher the absorption coefficient of X-ray and density than other elements in multi-

layer system, dominates the periodicity of reflectivity profiles (Figs. 4, 5). The fitting analysis (using WINGIXA program of Philips, Fig. 5) proved that the thickness of $IrMn_3$ remains unchanged and Al–O barrier decreases only slightly after annealing: from 15.5 Å for as-deposited sample to 14 Å for annealed one.

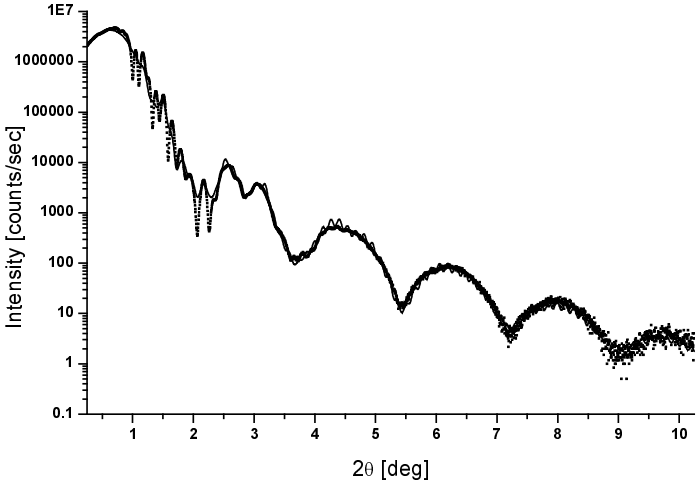

Fig. 5. θ–2θ reflectivity profile. Fitting profile (solid line) and experimental one (points)

The thickness of the top Ta layer increases by 8 Å (before annealing 55 Å, after – 63 Å) due to energetically preferred diffusion of Ni from the top electrode of $Ni_{80}Fe_{20}$ (high negative formation enthalpy of TaNi alloy, ΔH_{for}[TaNi] = –44kJ/mol) [24]. This conclusion is confirmed by the slight increase in the thickness (2 Å) of the bottom Ta layer (before annealing 47 Å, after 49 Å), because Cu from the adjacent layer does not diffuse into the bottom Ta layer due to negligibly small formation enthalpy (ΔH_{for}[TaCu] ≈ 0 kJ/mol) [24].

3.2. Tunneling magnetoresistance

The tunneling magnetoresistance was measured at RT in the cpp configuration (current perpendicular to the plane) with a four-point probe method for the sample annealed at 200 °C in magnetic field (1 kOe) with the electrode layer of $Ni_{80}Fe_{20}$ (1000 Å) deposited on the free layer of $Co_{70}Fe_{30}$ (25 Å). Figure 6 shows a typical high-field magnetoresistance hysteresis loop measured at RT for an annealed MTJ with the junction area of 250×250 μm^2. The major MR(H) loop originates from the magnetically hard electrode of $Co_{70}Fe_{30}$ (25 Å) pinned by the exchange biased coupling of antiferromagnetic $IrMn_3$ (100 Å) layer. The exchange biased field approaches H_{EB} of 1440 Oe. This value corresponds with unidirectional exchange biased energy 0.52 erg/cm^2 [22]. The minor MR(H) loop (as shown in Fig. 7) originates from the

free layer (top electrode) of $Co_{70}Fe_{30}$ (25 Å)/$Ni_{80}Fe_{20}$ (1000 Å). The coercive field of the free layer is about 3 Oe.

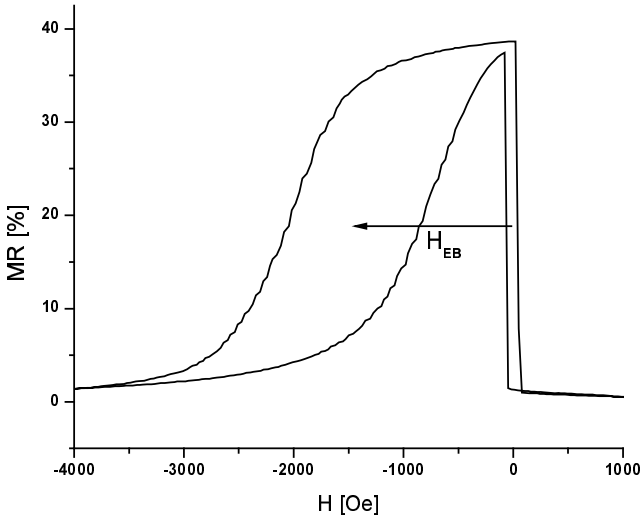

Fig. 6. High field MR-loop

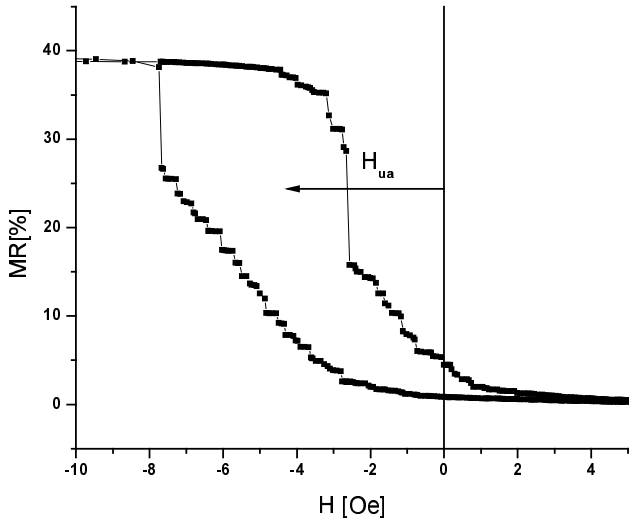

Fig. 7. Low field MR-loop

The minor loop is shifted about 5 Oe from zero magnetic field. The offset field (unidirectional anisotropy field H_{ua}), caused by the magnetic coupling between the pinned and free layers, has two components. The ferromagnetic coupling field, which is believed to result from the Néel "orange peel" coupling, is independent of the size of the junction and, on the other hand, the magnetostatic coupling which scales roughly in-

versely with the length of the junction is negligibly small, when the length of the pinned layer (i.e., the length of junction) is larger than 50 μm [20]. The minor MR(*H*) loop lies on the same side of the major MR(*H*) loop, indicating that the ferromagnetic "orange peel" coupling occurred between the free and pinned electrodes.

3.3. Local variation of magnetic parameters of free layer

In Figure 8, magnetooptical Kerr effect (MOKE) *M–H* loops are shown at several positions along the free-layer direction (the *y*-axis), as depicted in the inset of the figure. The *M–H* loop was measured under external magnetic field along the pinned-layer direction, i e. annealing field direction. There is no shift of the loop at the places located below the edge of the junction, as shown, for example, in Fig. 8. The shift due to the unidirectional anisotropy (bias) field H_{ua} increases as the measuring point moves to the junction centre, as shown in Figs. 8b–d, but then it decreases as the point moves away from the centre (Figs. 8e and f). One can also see a similar change of the coercive force H_c. Even though there are local variations of both H_c and H_{ua}, the squareness ratio of the loops is nearly constant.

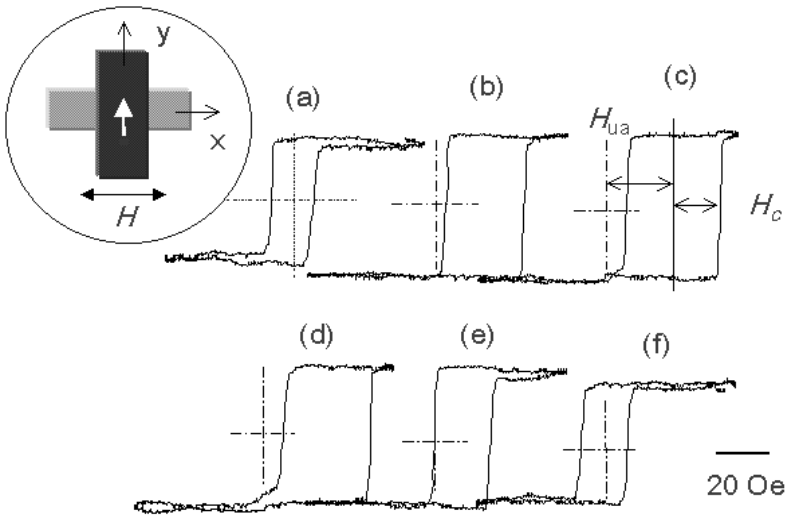

Fig. 8. MOKE *M–H* loops along the free-layer direction (the *y*-axis) at the positions:
0 (a), 105 (b), 130 (c), 165 (d), 205 (e), and 285 μm (f).
The starting point is 50 μm below the junction edge

Two-dimensional plots of maximum amplitude of the Kerr signal, obtained using a 20×20 scan, are shown in Figs. 9a, b for as-deposited and 200 °C-annealed junctions, respectively. The MOKE signal could be affected by the experimental parameters (e.g., the extinction coefficient of materials). Since the experimental parameters are fixed during the measurement, the maximum Kerr signal corresponds

with the maximum magnetization of a free layer. There is an irregular variation of the maximum Kerr signal in the as-deposited sample even near the centre of the free layer and also a gradual increase at the edge, and it reaches 90% of the centre value at 30 μm distance from the boundary. This variation is caused by the gradual change of film thickness (as shown in Fig. 10), arising from edge effects during deposition using a mask. After annealing, the irregular variation becomes smooth over the junction area except the edge region.

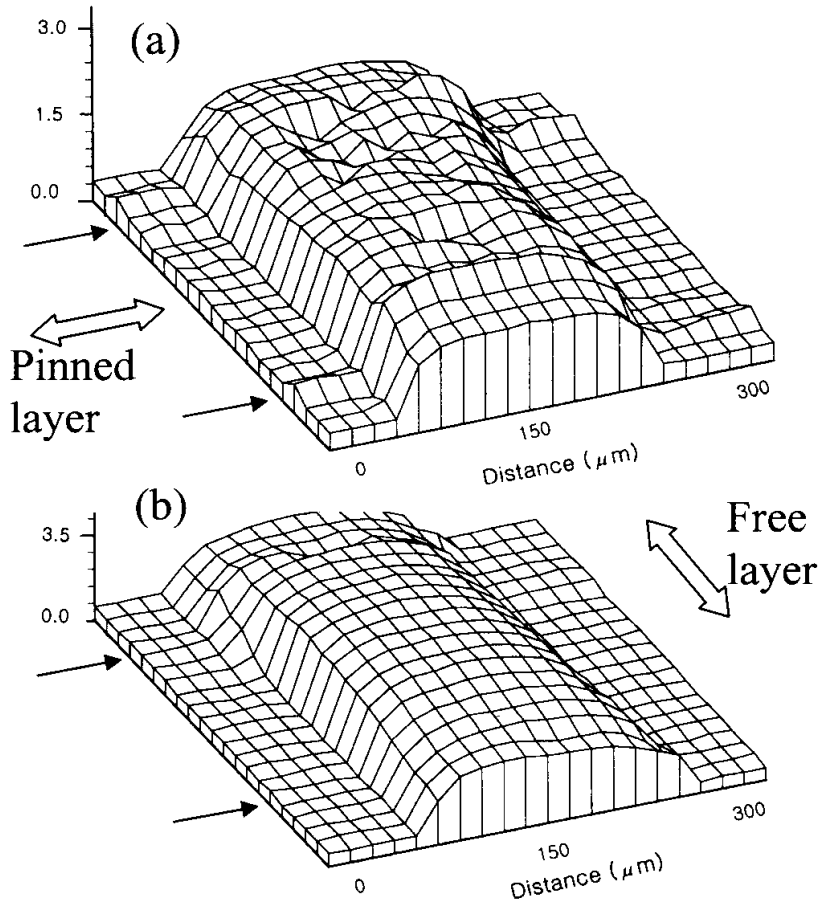

Fig. 9. Two-dimensional distribution of maximum magnetization in: as-deposited (a) and annealed (b) samples

The variations of H_c and H_{ua} for an annealed sample are compared with those for an as-deposited one in Figs. 11a, b, respectively. H_c in the as-deposited sample is about 10 Oe outside the junction with maximum of 17.5 Oe at the junction centre. The local changes of H_c are quite irregular, as shown in Fig. 11a. As a whole, H_c is reduced after field annealing, while the local variation becomes smooth and symmetric

with respect to the centre of junction. Figure 11b shows an irregular change of H_{ua} with the maximum of 7.5 Oe at the junction centre in the as-deposited sample.

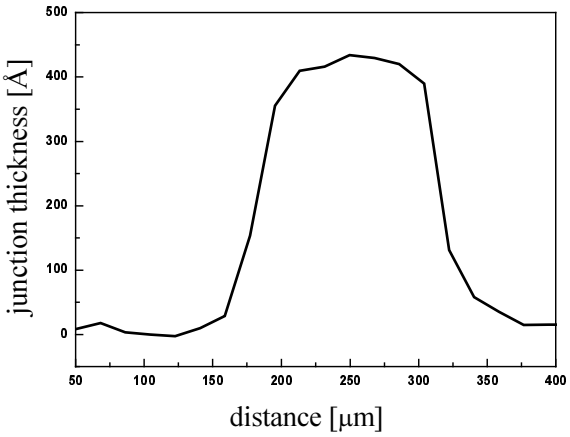

Fig. 10. α-step profile of the junction thickness

However, the field annealing enhances H_{ua} up to 20.5 Oe in the centre and, similarly to H_c variation, that of H_{ua} along the free layer becomes smooth (Fig. 11b). The enhancement of unidirectional anisotropy field and the smooth variations of H_{ua} and H_c after annealing are due to improvement of texture (111), increase of crystallites sizes, stress relaxation and alloying due to low-temperature diffusion [25].

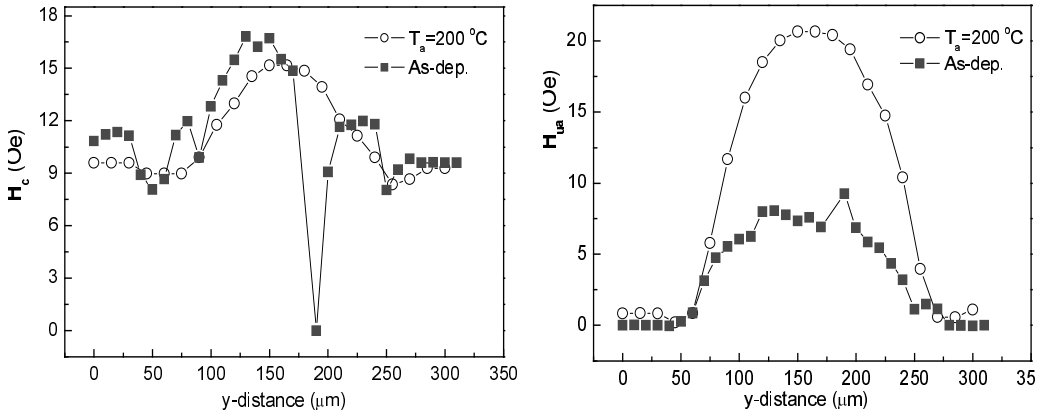

Fig. 11. Variation of coercive force H_c (a) and unidirectional bias field H_{ua} (b) along the free-layer axis in as-deposited and annealed samples

As we describe later, magnetic dipole interaction between the free and pinned layers is an origin of H_{ua}. Thus, the above described changes of H_{ua} might be influenced by the changes of the exchange biased anisotropy of pinned layer during field annealing [22].

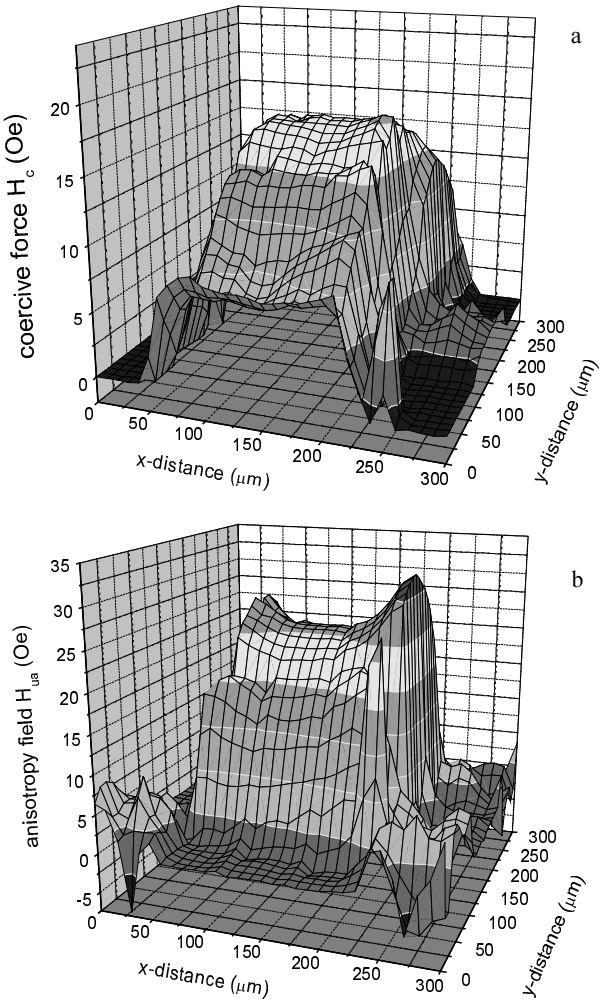

Fig. 12. Two-dimensional distribution of coercive force H_c (a) and unidirectional anisotropy field H_{ua} (b) in annealed sample: the *x*-axis: pinned layer, the *y*-axis: free-layer directions

In Figures 12a, b, two-dimensional plots of H_c and H_{ua}, respectively, are shown measured on the annealed sample, where measuring points are scanned over the entire junction area. Both H_c and H_{ua} show a saddle shape with its axis along the pinned-layer axis, where local variations along the pinned-layer axis are relatively small compared to those in the free-layer direction. As a whole, local variations of H_c and H_{ua} over the junction area are significant in comparison to the H_{ua} changes of magnetization (Fig. 9).

3.4. Surface roughness

Atomic force microscope (AFM) images across the pinned layer outside the junction are shown in Figs. 13a–d, at the measuring points *p*1–*p*4 depicted in the inset. At

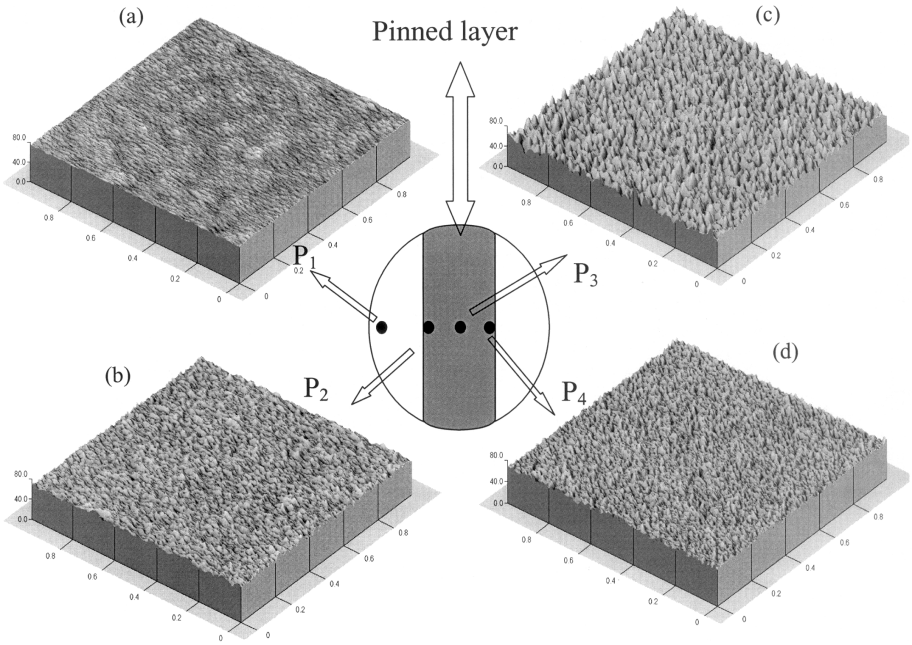

Fig. 13. AFM images across the pinned layer outside the junction: at the point *p*1, outside the layer (a); at point *p*2, near left edge (b); at point *p*3, centre (c) and at the point *p*4, near right edge (d). Scan area: 1×1 μm^2

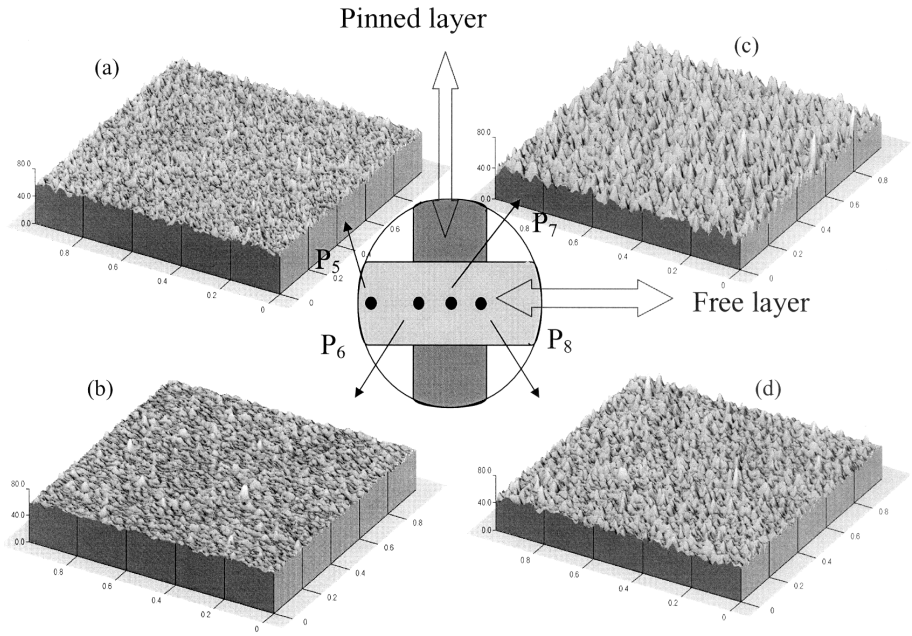

Fig. 14. AFM images along the free layer across the junction: at the point *p*5, outside the layer (a); at point *p*6, near left edge (b); at point *p*7, junction centre (c) and at the point *p*8, near right edge (d). Scan area: 1×1 μm^2

the point $p1$, outside the layer, the root mean square (RMS) roughness is 1.4 Å, corresponding to the surface roughness of the Si substrate. Within the layer, the roughness increases to 2.5 Å at $p2$ near the edge and to 5.5 Å at $p3$ near the centre of the layer, but then decreases to 2.7 Å near the left edge ($p4$).

In Figures 14a–d the AFM images are shown at several measuring points along the free layer across the junction. On the free layer outside the junction (point $p5$), RMS roughness is 3.3 Å, and becomes smaller, 2.3 Å at the near edge ($p6$). The roughness increases to 5.7 Å as the measuring point moves to the centre of the junction ($p7$), and then decreases as the point moves to the left edge ($p8$).

Figures 15a, b present the distribution of RMS roughness versus measuring distance, obtained from Figs. 13 and 14, respectively. The range of variation of RMS roughness is nearly the same (from 1.4 Å to 5.8 Å) and reveals symmetric variation with respect to the centre of the junction centre. However, the change near the edge is greater when roughness is measured on the free layer across the junction. These variations are quite similar to those of film thickness, as shown in the thickness profiles (given in Fig. 10). This may be a geometrical effect of the deposition process using a shadow mask.

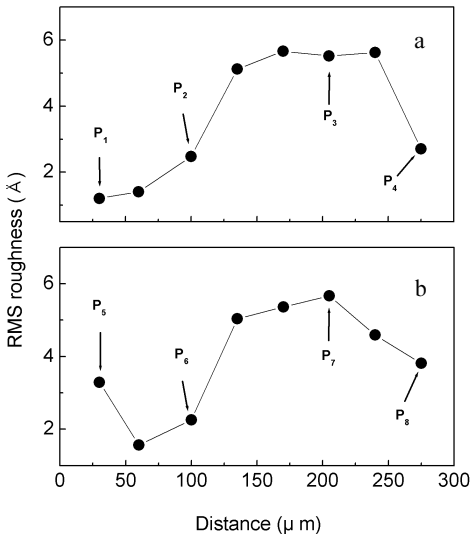

Fig. 15. Variation of average surface roughness across the pinned layer (a) and along the free layer across the junction (b)

In Figure 12, the H_{ua} distribution shape represents the exchange coupling field between free and pinned layers adjacent to the barrier of Al_2O_3. H_{ua} (~ 20 Oe) at the junction centre is about 4 times larger than that near the edge (~5 Oe). Ferromagnetic Néel's "orange peel" coupling by dipole interaction through tunneling barrier could be dominant over others such as RKKY-like interaction. In the Néel model,

a sinusoidal roughness profile is assumed and exchange coupling field H_N is expressed as [12]

$$H_N = \frac{\pi^2 h^2}{\sqrt{2} t_F \lambda} M_p \exp(-2\pi\sqrt{2} t_s / \lambda) \quad (1)$$

where h and λ are the amplitude and wavelength of the sinusoidal roughness profile, t_F and t_S are the thickness of the free layer and of the barrier layer, respectively, and M_p is the saturation magnetization of the pinned layer. Based on AFM measurement, the amplitude of the roughness profile is assumed to be 5.5 Å (RMS value at the junction centre). The wavelength of the roughness profile is reasonably assumed to be 100 Å as the grain diameter of the pinned $Co_{70}Fe_{30}$ layer as determined from XRD analysis [25]. Then, calculated from Eq. (1) the value of "orange peel" coupling is 22 Oe, being in reasonable agreement with the H_{ua} value at the junction centre.

M_p could be constant irrespective of the pinned layer thickness. When the thickness t_F is taken into account in denominator, the increase of H_{ua} at both edges, determined from measurements outside the junction, across the pinned layer (along the *y*-direction, Fig. 12b) where the roughness amplitude is small in relation to the centre (Figs. 13 and 15a), is described well by the decrease of t_F at the edges. But H_{ua} (Figs. 11b and 12b, along the *x*-direction), determined from the measurements inside the junction across the free layer, increases due to increasing roughness amplitude from the edge to the centre of junction (Figs. 14 and 15b). Because the exchange coupling field is given as a square function of the roughness amplitude h, the coupling at the junction centre along free layer is expected to be 4–5 times higher than that near the edge from the roughness shown in Figs. 14 and 15b. There is a good agreement between the measured and expected H_{ua} variations, suggesting that H_{ua} in the free layer is well described by dipole interaction between the free and pinned layers.

4. Conclusions

We have discussed the local variation of magnetization, coercive force and unidirectional anisotropy field of the free layer of MTJs in as-deposited and annealed samples. The XRD analysis revealed that highly oriented *fcc* (111) crystal planes of $IrMn_3$, Cu, $Ni_{80}Fe_{20}$ and $Co_{70}Fe_{30}$ grow parallel to the substrate plane. The annealing treatment improved the crystallinity and texture in the samples investigated which lead to smoother distributions of magnetization H_{ua} and H_c in annealed junction in comparison to as-deposited ones. Unidirectional anisotropy field H_{ua} should be uniform over the junction area when the thickness alone is taken into account in dipole interactions. However, roughness is also involved in dipole interactions, so the coupling at the junction centre is expected to be 4–5 times higher than that near the edge. There is a good agreement between the measured and expected H_{ua} variations, sug-

gesting that H_{ua} of the free layer is well described by dipole interaction in the term of Néel "orange-peel" coupling between the free and pinned layers. As a whole, the reversal magnetization is not uniform over the entire junction area and macroscopic properties are governed by the averages of the local distributions.

References

[1] MIYAZAKI T., TEZUKA N., J. Magn. Magn. Mater., 139 (1995), L231.
[2] MOODERA J.S., KINDER L.R., WONG T.M., MESERVEY R., Phys. Rev. Lett., 74 (1995), 3273.
[3] TSUNODA M., NISHIKAWA K., OGATA S., TAKAHASHI M., Appl. Phys. Lett., 80 (2002), 3135.
[4] PARKIN S.S.P., ROCHE K.P., SAMANT M.G., RICE P.M., BEYERS R.B., SCHEUERLEIN R.E., O'SULLIVAN E.J., BROWN S.L., BUCCHIGANO J., ABRAHAM D.W., LU YU, ROOKS P.L., TROUILLOUD M., WANER R.A., GALLAGHER W.J., J. Appl. Phys., 85 (1999), 5828.
[5] RICHTER R., BÄR L., WECKER J., REISS G., Appl. Phys. Lett., 80 (2002), 1291.
[6] MILLER M.M., SHEEHAN P.E., EDELSTEIN R.L., TAMANAHA C.R., ZHONG L., BOUNNAK S., WHITMAN L.J., COLTON R.J., J. Magn. Magn. Mat., 225 (2001), 138.
[7] SCHOTTER J., KAMP P.B., BECKER A., PÜHLER A., BRINKMANN D., SCHEPPER W., BRÜCKL H., REISS G., IEEE Trans. Magn., 38 (2002), 3365.
[8] SONG D., NOWAK J., LARSON R., KOLBO P., CHELLEW R., IEEE Trans. Magn., 36 (2000), 2545.
[9] JULLIERE M., Phys. Lett., 54A (1975), 225.
[10] SLONCZEWSKI J.C., Phys. Rev., B39 (1989), 6995.
[11] RUDERMAN M.A., KITTEL C., Phys. Rev., 96 (1954), 99.
[12] NÉEL L., C.R. Acad. Sci., 255 (1962), 1676.
[13] LEE C., BAIN J.A., CHU S., MCHENRY M.E., J. Appl. Phys., 91 (2002), 7113.
[14] STOBIECKI F., STOBIECKI T., OCKER B., MAASS W., POWROZNIK W., PAJA A., LOCH C., RÖLL K., Acta Phys. Polon., (A), 97 (2000), 523.
[15] MIURA S., TSUNODA M., TAKAHASHI M., J. Appl. Phys., 89 (2001), 6308.
[16] SHEN J.X., KIEF M.T., J. Appl. Phys., 79 (1996), 5008.
[17] PARK C.M., MIN K.I., SHIN K.H., IEEE Trans. Magn., 32 (1996), 3422.
[18] HOU C., CHEN J., KIEF M.T., GAO Z., MAO S., POKHIL T., Appl. Phys. Lett., 78 (2001), 237.
[19] HOU C., FUJIWARA H., UEDA F., J. Magn. Magn. Mater., 198–199 (1999), 450.
[20] SCHRAG B.D., ANGUUELOUCH A., XIAO G., TROUILLOUD P., LU YU, GALLAGHER W.J., PARKIN S.S.P., J. Appl. Phys., 87 (2000), 4682.
[21] LI K., WU Y., QIU J., HAN G., GUO Z., CHONG T., J. Magn. Magn. Mat., 241 (2002), 89.
[22] TSUNODA M., TSUCHIYA Y., HASHIMOTO T., TAKAHASHI M., J.Appl. Phys., 87 (2000), 4375.
[23] ANDERSON G., HUAI Y., MILOSLAWSKY L., J. Appl. Phys., 87 (2000), 6989.
[24] SCHMALHORST J., BRUECKL H., REISS G., GIERES G., WECKER J., J. Appl. Phys., 91 (2002), 6617.
[25] STOBIECKI T., KANAK J., KIM C.G., to be published.

Received 4 December 2002
Revised 31 January 2003